Preprints (www.preprints.org) | NOT PEER-REVIEWED | Posted: 3 October 2022 doi:10.20944/preprints202210.0007.v1

Article

Optimal Propellant-less Control of a Solar Sail

Andre Pittella [1], Timothy Sands [1]

[1] Sibley School of Mechanical and Aerospace Engineering, Cornell University; ap826@cornell.edu

Abstract: Solar sails use radiation from the sun to generate thrust without any fuel or propellant. Since this is a form of propulsion that has theoretically infinite use, we would like to test its capability on long-term missions by simulating a spacecraft equipped with solar sails to the Sun-Earth L5 Lagrange point. To control the sail angle, which is the main form of control we have over the sail's performance, we will devise a form of optimal control based on Pontryagin's Minimum Principle. Simulating the dynamics in MATLAB SIMULINK, we find that such a control method relies on iterating over initial conditions for the co-states to find the necessary parameters for the trajectory to reach the desired point. Therefore, an autonomous control scheme that uses this form of optimal control will need a way to numerically find said initial conditions in order to find the control angle needed at any point in time, which may be computationally intensive.

Keywords: optimal control; solar sails; Lagrange points; Pontryagin's Principle

1. Introduction

Theorized first in the early 20th century, solar sails were first successfully deployed in 2010 with the launch of the Japan Aerospace Exploration Agency's IKAROS spacecraft, which used a square-shaped solar sail to navigate to Venus over the course of six months. Solar sails lack the fine directional and intensity control of typical fuel/propellant propulsion sources, as the only control on a sail is its angle relative to the incoming sunlight, which will affect both the strength of the thrust and its direction simultaneously. However, there is no cost associated with the 'amount' of control to apply compared to the fuel budgets of other propulsion sources, so designing trajectories using solar sails is done with finding the minimal time for trajectories that are as accurate as possible.

Lagrange points are points in a 3-body gravitational system where the gravitational potential energy has a minimum or maximum, leading to equilibriums of varying stability. These points are found using the circular restricted 3-body problem (CR3BP), an accurate approximation of 3-body systems found in the solar system. [1] For the Sun-Earth system, the L5 point is stable, and forms an equilateral triangle with the Sun and Earth. Paths within the CR3BP are characterized by their associated Jacobi Constant, which reflects the conservation of energy within the non-inertial barycentric frame of the CR3BP. [2] Non-gravitational forces such as those of propulsion can raise or lower the Jacobi Constant, which may indicate the future paths the spacecraft in question may settle on.

Many solutions have been developed [3] including proposed updates to classical approaches in [4], and also including optimal analytic methods for simple cases [5, 6] while optimal methods guiding and controlling realistic nonlinear systems ubiquitously necessitate either computational solutions or linearization to achieve analytical solutions. The literature is abound with debates over classical versus modern approaches and analytic versus numerical approaches, and those debates continue in this manuscript.

This manuscript proposes techniques for seeking optimization solutions to the full, nonlinear, coupled equations of mechanical motion.

Rao proposed numerical trajectory optimization applied to orbital transfer problems [7] but also produced a survey of numerical methods for optimal control [8]. Numerical methods are very quicky resorted to as researchers grapple with six nonlinear, coupled

© 2022 by the author(s). Distributed under a Creative Commons CC BY license.

Preprints (www.preprints.org) | NOT PEER-REVIEWED | Posted: 3 October 2022 doi:10.20944/preprints202210.0007.v1

equations of mechanical motion (both translation and rotation). A generalized treatment method (again numerical) as optimization problems was proposed in [9] for such orbital transfer problems, spacecraft rendezvous and docking [10-12], and planetary entry and hypersonic space planes [13–17]. Gan [13] and Rajesh [15] proposed using the genetic algorithm for reentry vehicle trajectory optimization, while Kenan [14] utilized pseudo-spectral numerical optimization. Robert [16] applied energy-state approximation techniques to design trajectories that minimized heat load on the re-entry vehicle, while Mikhail proposed and engineering local bridging method (computational).

The analytic methods were meanwhile demonstrated effective even on multi-body flexible space robotics in [18] where critical comparative analysis was recently presented in [19]. Arguably, following the publication of [20], numerical optimization in general form realized the current dominance of numerical methods, e.g. [21,22] for real-time (numerical) trajectory optimization, [23, 24] for aero-assisted optimal tracking guidance. Despite the current emphasis in the literature on numerical approaches, Sandberg [25] compared analytic optimal trajectory optimization by Pontryagin's method to classical optimization via regression parameterization, while Raigoza [26] quickly followed with augmentation of autonomous collision avoidance. This manuscript constitutes extension of the methods to six-degree-of-freedom coupled motion of a solar sail navigation with no propulsion.

2. Materials and Methods

2.1 Circular Restricted 3-Body Problem

The circular restricted 3-body problem (CR3BP) is a simplification of the dynamics of a 3-body gravitational system that allows for easy simulation and analysis of a body being gravitationally attracted to 2 bodies at once, whose respective masses are large enough that the third body's effect on them is negligible. The problem is drawn up in a rotating, barycentric frame, so that the 2 massive bodies are in fixed positions and the free body moves around in the plane of the system. Additionally, there are several unit changes to simplify analysis. If m_1, m_2 are the masses of the two greater bodies, $\boldsymbol{r}_{1/2}$ is the position of the larger body relative to the smaller, and $T_{1,2}$ is the period of the two greater bodies, then these are:

$$m_1 + m_2 = 1\ MU \tag{1}$$

$$\left|\boldsymbol{r}_{1/2}\right| = 1\ DU \tag{2}$$

$$T_{1,2} = 2\pi\ TU \tag{3}$$

These expressions define the mass units (MU), distance units (DU), and time units (TU) of the CR3BP. We will write

$$m_2 = \mu^*, m_1 = 1 - \mu^* \tag{4}$$

so that both masses can be defined from the same original parameter, which is roughly equal to the ratio of masses of the system:

$$\frac{m_2}{m_1} = \frac{\mu^*}{1-\mu^*} \approx \mu^*(1+\mu^*) = \mu^* + \mu^{*2} \tag{5}$$

which reduces to μ^* if $\mu^* \ll 1$. If the origin of the system *O* is the barycenter of the greater masses, then we can write their positions knowing that the barycenter is the center of mass. The CR3BP frame is defined such that all orbits are confined to one plane, and the two greater bodies are on co-circular orbits such that, in the rotating frame, they stay fixed on the horizontal *x* axis. Thus,

$$\boldsymbol{r}_{1/O} = -\mu^*\hat{\boldsymbol{x}} \tag{6}$$

Preprints (www.preprints.org) | NOT PEER-REVIEWED | Posted: 3 October 2022 doi:10.20944/preprints202210.0007.v1

$$\boldsymbol{r}_{2/O} = (1-\mu^*)\hat{\boldsymbol{x}} \tag{7}$$

This, combined with the rotation of the CR3BP frame and taking the gravitational constant $G = 1$, yields the acceleration of a body at point (x, y) due to gravity as well as the Coriolis effect & centripetal forces:

$$a_x = 2\dot{y} + x - \frac{(1-\mu^*)x}{((x+\mu^*)^2+y^2)^{\frac{3}{2}}} - \frac{\mu^* x}{((x+\mu^*-1)^2+y^2)^{\frac{3}{2}}} \tag{8}$$

$$a_y = -2\dot{x} + y - \frac{(1-\mu^*)y}{((x+\mu^*)^2+y^2)^{\frac{3}{2}}} - \frac{\mu^* y}{((x+\mu^*-1)^2+y^2)^{\frac{3}{2}}} \tag{9}$$

where dots denote a derivative in time. The potential energy of the CR3BP is given by

$$U = -\frac{1}{2}(x^2+y^2) - \left(\frac{1-\mu^*}{r_1} + \frac{\mu^*}{r_2}\right) \tag{10}$$

so that equilibrium points, also called Lagrange points, are found when

$$\frac{\partial U}{\partial x} = -\frac{\mu^*(-\mu^*-x+1)}{r_2^3} - x - \frac{(1-\mu^*)(-\mu^*-x)}{r_1^3} = 0 \tag{11}$$

$$\frac{\partial U}{\partial y} = \frac{\mu^* y}{r_2^3} - y + \frac{y(1-\mu^*)}{r_1^3} = 0 \tag{12}$$

The solution of these constraints for non-zero y component yields that the distance of the free body from both massive bodies is simultaneously 1, meaning the three bodies draw out an equilateral triangle. L4 and L5 are the two points which make these triangles, one which leads the Earth's orbit, and one which lags behind. We will choose L5, that which lags behind, with the position in the CR3BP frame of

$$x_{L5} = \frac{1}{2} - \mu^*, y_{L5} = -\frac{\sqrt{3}}{2} \tag{13}$$

2.2 Solar Sail Dynamics

For a finite solar sail with area A, mass m, and reflectivity ρ, the acceleration due to the force of solar radiation pressure is given by

$$\boldsymbol{a} = \frac{p_0}{r_1^2}\left(\frac{A}{m}\right)\cos\delta\left((1-\rho)\boldsymbol{l} + 2\rho\cos\delta\,\boldsymbol{n}\right) \tag{14}$$

where δ is the angle the sail's normal vector $\boldsymbol{n}$ makes with the incident light direction vector $\boldsymbol{l}$. [1] p_0 is the solar radiation pressure measured at Earth, and r_1 is defined as previously, the distance between the body and the greater mass in DU, which in this case is the Sun and the distance units are equal to astronomical units.

The components of the two unit vectors above are given by

$$\boldsymbol{l} = [\cos\theta \;\; \sin\theta \;\; 0]^T \tag{15}$$

$$\boldsymbol{n} = [\cos(\theta+\delta) \;\; \sin(\theta+\delta) \;\; 0]^T \tag{16}$$

where θ is the angle that the body's position vector makes with the horizontal axis.

For a solar sail made of Mylar, which we will simulate, the areal loading is 7 g/m^2, which gives a figure for A/m of about 140 m^2/kg. Additionally, the reflectivity ρ is approximately 0.9.

Pontryagin's Maximum Principle

For the state-space problem formulation of

$$\dot{x} = f\big(x(t), u(t)\big) \tag{17}$$

Preprints (www.preprints.org) | NOT PEER-REVIEWED | Posted: 3 October 2022 doi:10.20944/preprints202210.0007.v1

$$J = \phi\left(x_{t_f}, t_f\right) + \int_{t_0}^{t_f} L(x(t), u(t), t)\, dt \tag{18}$$

the Hamiltonian can be constructed using the costate vector λ:

$$H = \lambda^T f(x, u) + L(x, u, t) \tag{19}$$

Pontryagin's Minimum Principle states that the optimal state trajectory x^*, control u^*, and costate vector λ^* must minimize the Hamiltonian at all times, such that

$$H(x^*, u^*, \lambda^*, t) \leq H(x^*, u, \lambda^*, t) \tag{20}$$

Additionally, to minimize the cost functional J over the time span of (t_0, t_f), additional constraints must be met:

$$\dot{\lambda}^T(t) = -\frac{\partial H}{\partial x} \tag{21}$$

$$\lambda^T\left(t_f\right) = \frac{\partial \phi}{\partial x}\Big|_{t=t_f} \tag{22}$$

To formulate the problem being simulated, our state will be

$$\boldsymbol{x} = \left[x\ y\ v_x\ v_y\right]^T \tag{23}$$

with desired state

$$\boldsymbol{x}(t_f) = \left[\frac{1}{2} - \mu^*\ \frac{\sqrt{3}}{2}\ \ 0\ \ 0\right]^T \tag{24}$$

which is synonymous with being at rest at the L5 Lagrange Point [2]. The first two state variables indicate the position in the CR3BP rotating frame, and the second two are the velocity components in the same frame. As we desire a time-optimal trajectory to a known location, the cost functional is constructed using

$$\phi\left(x_{t_f}, t_f\right) = \frac{1}{2}\left[\left(x - \frac{1}{2} + \mu^*\right)^2 + \left(y - \frac{\sqrt{3}}{2}\right)^2\right] \tag{25}$$

$$L = 1 \tag{26}$$

On paper, the Minimum Principle can be solved to yield analytical equations for an optimal control. However, due to the many nonlinearities in the system dynamics, this will not be possible. However, seeing how the mathematical constraints flow together, we can piece together a numerical algorithm that can be iterated to find an optimal solution. Since there is no equation that uses the initial values of the costate, we try a set of values at the beginning of the simulation. Using the state and costate, the simulation will then find the control angle that minimizes the Hamiltonian. Afterwards, the state and costate are propagated forward in time using numerical integration, as both their derivatives in time are known. As this algorithm does not take into account the desired final state, different values for the costate initial conditions must be tried to settle on one that best reaches the desired final state.

3. Results

The following simulations were performed in MATLAB SIMULINK, using the ode45 integrator and a maximum step size of 0.0001. To show the range of trajectories possible, the result of integrating the initial conditions with no solar sail thrust as well as maximum thrust are shown afterwards. The initial position and velocity of the spacecraft is chosen to both fit realistic values from a launch vehicle and to allow a range of trajectories that includes the desired point.

Preprints (www.preprints.org) | NOT PEER-REVIEWED | Posted: 3 October 2022 doi:10.20944/preprints202210.0007.v1

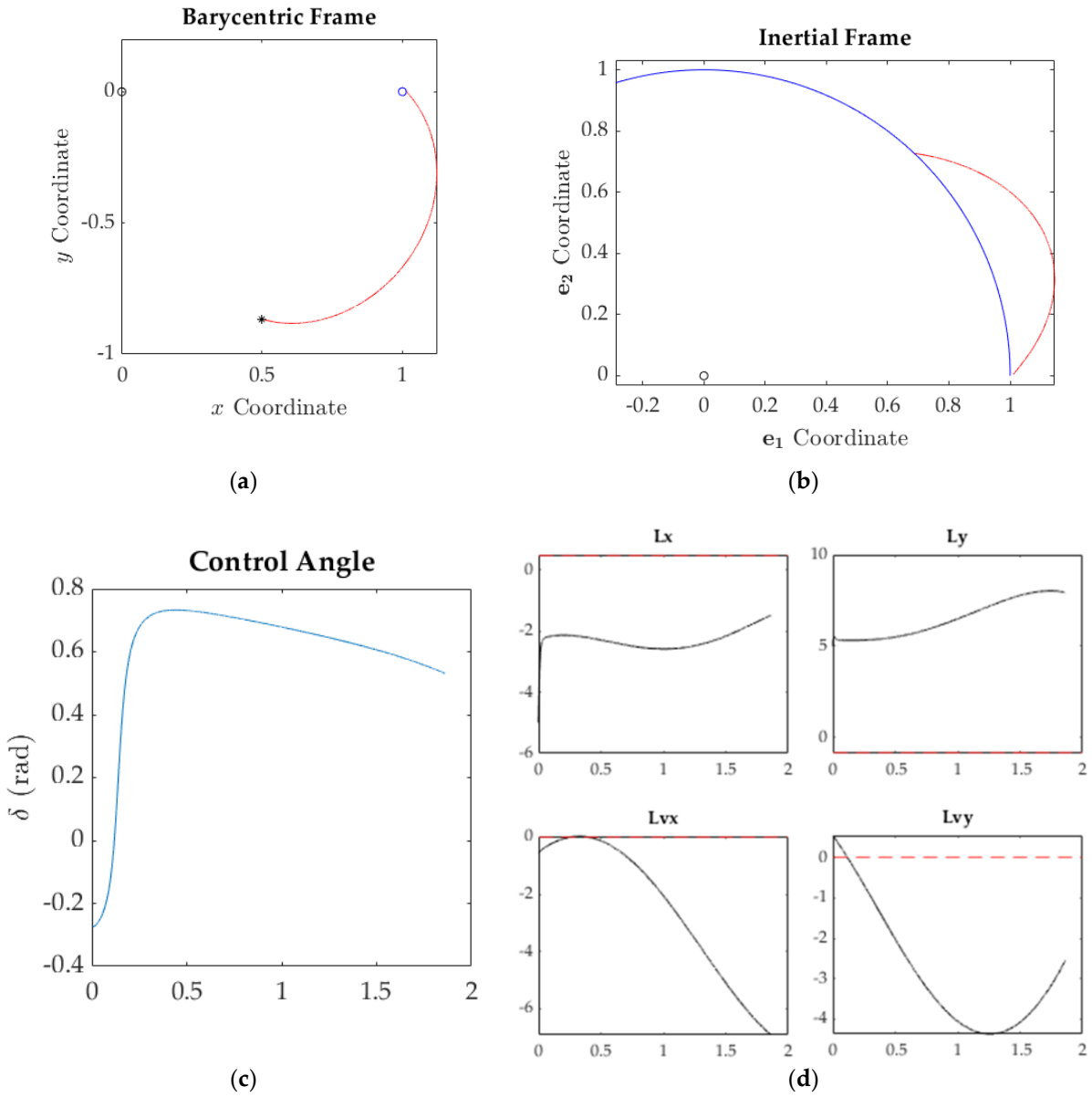

Figure 1. Simulation plots. **a)** The motion of a solar sail spacecraft in the rotating CR3BP frame. Black circle represents the position of the Sun, the blue circle the Earth, the asterisk the L5 Lagrange point, and the red line is the spacecraft trajectory. **b)** The same trajectory, represented in an inertial frame, with the blue line representing the Earth's motion around the Sun. **c)** The optimal control angle over time as calculated using Pontryagin's Minimum Principle. The horizontal axis is in time units (TU), with 1 TU = 0.159 years. **d)** The evolution of the costate components over time. Red dashed lines show the final values for the costate components according the Minimum Principle.

Preprints (www.preprints.org) | NOT PEER-REVIEWED | Posted: 3 October 2022 doi:10.20944/preprints202210.0007.v1

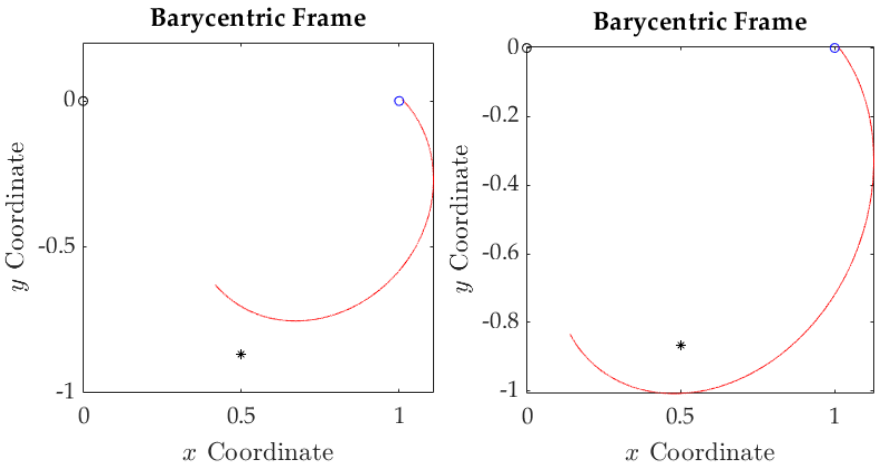

Figures 2 & 3. Simulation plots. **2:** The trajectory of the spacecraft without using any solar sa thrust, i.e. purely gravitational flight. **3:** The trajectory of the spacecraft with maximum sol sail thrust, i.e. $\delta = 0$ and the sails are directed normal to the sunlight.

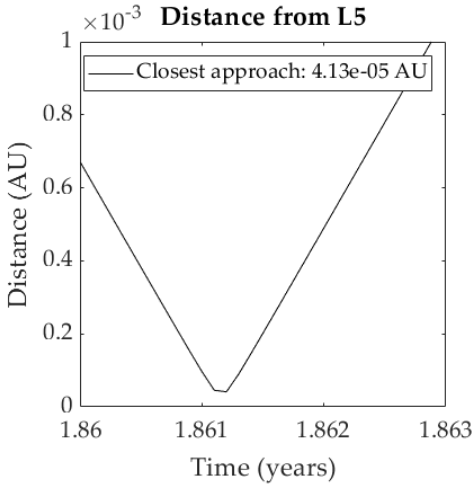

Figures 4. Plot showing the approach distance from the desired final point.

4. Discussion

From the results in Section 3, we can see that with the initial costate components of equation (27)

$$\lambda(t_0) = [-5 \quad 5 \quad -0.5473 \quad 0.5473]^T \tag{27}$$

put the spacecraft on a path that leads to the desired Lagrange point, L5. The trip takes 1.86115 TU, or 0.2962 years. However, the spacecraft is unable to stop entirely at L5 like the desired state requires. This can be seen in Figure 4, as the spacecraft begins to gain distance from L5. Additionally, we can see from Figure 1d that the co-states do not converge on the final values necessitated by the Minimum Principle. Comparing the magnitudes of forces acting on the spacecraft, it is unlikely that the spacecraft will be able to slow itself down upon arrival to the Lagrange point with just solar sails. However, reaching the point itself can be considered a minor success as the spacecraft can be equipped with some kind of other propulsion source that can enact a burn right at L5 to instantaneously correct the velocity to stay at L5.

An improvement to this control method would be to numerically iterate over many different initial costate vectors and isolate those which come within a certain range of L5 at some point in their trajectory. Finding a working initial costate was done by hand. To conserve computation time, the simulations for every combination of initial values should

be done over relatively coarse time spans. As the computer finds a combination with the fastest approach time to L5, it will then increase the time steps and explore the coordinate space around the initial costate, eventually settling on a 'best' initial costate.

Another control method that is not based in any optimality theory is to use the control angle in which the resulting solar sail's thrust force has the largest component possible along a vector connecting the spacecraft's position and the position of the desired final position, or using the control angle in which the *resultant* force acting on the spacecraft, that is, gravity as well as the solar sail thrust force, has the biggest component pointing towards the desired point.

5. Conclusions

Because finding a trajectory required human iteration, using Pontryagin's Minimum Principle directly to find a control for this problem is ultimately not recommended. Although the simulation has the spacecraft reaching the L5 Lagrange point, it comes in at a non-zero velocity, which is not equivalent to the desired state, which has zero velocity in the rotating CR3BP frame. A recommended improvement of this control scheme would be making the code iterate over many initial conditions for the costate vector, or perhaps changing the physical parameters of the solar sail, such as the area to mass ratio, to allow for greater thrust to allow the sail to slow the spacecraft to a complete halt. Additionally, orbits around L5 that qualify as 'horseshoe' or 'tadpole' orbits may be possible for approaches within limited velocity regimes. More mathematically complex solution algorithms exist, such as pseudospectral methods [3].

Author Contributions: Conceptualization, A.P. and T.S.; methodology, A.P. and T.S.; software, A.P.; validation, A.P. and T.S.; formal analysis, A.P.; investigation, A.P.; resources, T.S; data curation, A.P.; writing—original draft preparation, A.P.; writing—review and editing, A.P. and T.S.; visualization, A.P..; supervision, T.S; project administration, T.S.; funding acquisition, T.S.. All authors have read and agreed to the published version of the manuscript. Please turn to the CRediT taxonomy for the term explanation. Authorship has been limited to those who have contributed substantially to the work reported.

Funding: Please add: This research received no external funding. APC was funded by the corresponding author.

Conflicts of Interest: The authors declare no conflict of interest.

References

1. Koblik, Viacheslav & E, Polyakhova & Sokolov, Leonid. Solar sail near the Sun: Point-like and extended models of radiation source. *Advances in Space Research.* **2011**, *48*. 10.1016/j.asr.2011.04.024.
2. Heiligers, J., Fernandez, J. M., Stohlman, O. R., & Wilkie, W. K. Trajectory Design for a Solar-Sail Mission to Asteroid 2016 HO3. *Astrodynamics* **2019**, *3*(3), 231–246. https://doi.org/10.1007/s42064-019-0061-1.
3. Sands, T. Treatise on analytic nonlinear optimal guidance and control. *Frontiers in Robotics and AI* **2022**, *9* 10.3389/frobt.2022.884669. Available online (accessed 30 Sep 2022): https://www.frontiersin.org/articles/10.3389/frobt.2022.884669/abstract. Also available at: doi: 10.20944/preprints202201.0467.v1.
4. Baker, K., Cooper, N., Heidlauf, P., Sands, T. Autonomous Trajectory Generation for Deterministic Artificial Intelligence, *Electrical and Electronic Engineering*, **2018**, *8*(3), 59-68. doi: 10.5923/j.eee.20180803.01.
5. Fahroo, F., & Ross, I. M. (n.d.). (rep.). Advances in Pseudospectral Methods for Optimal Control. Proceedings of AIAA Guidance, Navigation and Control Conference, Honolulu, Hawaii USA, August 18–21, 2008.
6. Chaia,R.; Savvarisa, A.; Tsourdosa, A.; Tsourdos, A.; Chai, S.; Xia, Y. A review of optimization techniques in spacecraft flight trajectory design. *Progress in Aerospace Sciences* **2019**, *109*(2). Doi: 10.1016/j.paerosci.2019.05.003.
7. Rao, A.; Tang, S.; Hallman, W. Numerical optimization study of multiple-pass aero assisted orbital transfer, *Optimal Control Applications and Methods* **2002**, *23*(4), 215–238. doi:10.1002/oca.711.
8. Rao, A. A survey of numerical methods for optimal control, *Advances in the Astronautical Sciences* **2009**, *135*(1), 497-528.
9. Ross, I. M.; Karpenko, M. A review of pseudospectral optimal control: From theory to flight, *Annual Reviews in Control* **2012**, *36*(2), 182–197. doi: https://doi.org/10.1016/j.arcontrol.2012.09.002.
10. Gao, H.; Yang, X.; Shi, P. Multi-objective robust h-infinity control of spacecraft rendezvous, *IEEE Transactions on Control Systems Technology* **2009**, *17*(4) 794–802. doi:10.1109/TCST.2008.2012166
11. Bonnans, J.; Festa, A. Error estimates for the Euler discretization of an optimal control problem with first-order state constraints, *SIAM Journal on Numerical Analysis* **2017**, *55*(2) 445–471. doi:10.1137/140999621.

Preprints (www.preprints.org) | NOT PEER-REVIEWED | Posted: 3 October 2022 doi:10.20944/preprints202210.0007.v1

12. Pontani, M.; Conway, B. Optimal finite-thrust rendezvous trajectories found via particle swarm algorithm, *Journal of Spacecraft and Rockets* **2013**, *50*(6), 1222–1234. doi:10.2514/1.A32402.
13. Gan, C.; Zi-ming, W.; Min, X.; Si-lu, C. Genetic Algorithm Optimization of RLV Reentry Trajectory, In Proceedings of the AIAA/CIRA 13th International Space Planes and Hypersonic Systems and Technologies Conference, Capua, Italy, 16-20 May 2005. doi:10.2514/6.2005-3269.
14. Kenan, Z.; Wanchun, C. Reentry Vehicle Constrained Trajectory Optimization, In Proceedings of the 17th AIAA International Space Planes and Hypersonic Systems and Technologies Conference, San Francisco, California, 11-14 April 2011. doi:10.2514/6.2011-2231.
15. Rajesh, A. Reentry Trajectory Optimization: Evolutionary Approach, In Proceedings of the 9th AIAA/ISSMO Symposium on Multidisciplinary Analysis and Optimization, Atlanta, Georgia, 4-6 September 2002. doi:10.2514/6.2002-5466.
16. Robert, W.; Mark, A. Jeffrey, B.; Robert, W.; Mark, A.; Jeffrey, B. Minimum heating reentry trajectories for advanced hypersonic launch vehicles, In Proceedings of the Guidance, Navigation, and Control Conference, New Orleans, LA, U.S.A. 11-13 August 1997. doi: 10.2514/6.1997-3535.
17. Mikhail, I.; Pavel, V.; Alexandr, K. Numerical Investigation of the EXPERT Reentry Vehicle Aerothermodynamics Along the Descent Trajectory, In Proceedings of the 39th AIAA Thermophysics Conference, Miami, Florida, 25-28 June 2007. doi:10.2514/6.2007-4145.
18. Sands, T. Optimization Provenance of Whiplash Compensation for Flexible Space Robotics. *Aerospace* **2019**, *6*, 93. https://doi.org/10.3390/aerospace6090093
19. Sands, T. Flattening the Curve of Flexible Space Robotics. *Appl. Sci.* **2022**, *12*, 2992. https://doi.org/10.3390/app12062992
20. Ross, M. *A primer on Pontryagin's principle in optimal control*, CA: Collegiate Publishers, **2015**.
21. Tian, B.; Fan, W.; Su, R.; Zong, Q. Real-time trajectory and attitude coordination control for reusable launch vehicle in reentry phase, *IEEE Transactions on Industrial Electronics* **2015**, 62(3), 1639–1650. doi:10.1109/TIE.2014.2341553.
22. Sagliano, M.; Mooij, E.; Theil, S. Onboard trajectory generation for entry vehicles via adaptive multivariate pseudospectral interpolation, *Journal of Guidance, Control, and Dynamics* **2017**, *40*(2), 466–476. doi:10.2514/1.G001817.
23. R. Chai, A. Savvaris, A. Tsourdos, S. Chai, Y. Xia, Optimal tracking guidance for aeroassisted spacecraft reconnaissance mission based on receding horizon control, *IEEE Transactions on Aerospace and Electronic Systems* **2018**, *54*(4), 1575–1588.
24. Chai, R,; Savvaris, A.; Tsourdos, A.; Chai, S.; Xia, Y. Optimal fuel consumption finite-thrust orbital hopping of aeroassisted spacecraft, *Aerospace Science and Technology* **2018**, 75, 172–182. doi:https://doi.org/10.1016/j.ast.2017.12.026.
25. Sandberg, A.; Sands, T. Autonomous Trajectory Generation Algorithms for Spacecraft Slew Maneuvers. *Aerospace* **2022**, *9*, 135. https://doi.org/10.3390/aerospace9030135
26. Raigoza, K.; Sands, T. Autonomous Trajectory Generation Comparison for De-Orbiting with Multiple Collision Avoidance. *Sensors* **2022**, *22*, 7066. https://doi.org/10.3390/s22187066